Received: 24 June 2020 | Revised: 1 October 2020 | Accepted: 20 October 2020

IET Generation, Transmission & Distribution

DOI: 10.1049/gtd2.12068

The Institution of Engineering and Technology WILEY

ORIGINAL RESEARCH PAPER

A novel AC line distance protection scheme for AC/DC hybrid system based on fault likeness factor

Jing Ma[1] | **Yuchong Wu**[1] | **Arun G. Phadke**[2]

[1] State Key Laboratory of Alternate Electrical Power System with Renewable Energy Sources, North China Electric Power University, Beijing, China

[2] Bradley Department of Electrical and Computer Engineering, Virginia Polytechnic Institute and State University, Blacksburg, Virginia, USA

Correspondence
Jing Ma, State Key Laboratory of Alternate Electrical Power System with Renewable Energy Sources, North China Electric Power University, Beijing 102206, China.
Email: corresponding.hdmajing@163.com

Funding information
National Natural Science Foundation of China, Grant/Award Number: 51822703; Chinese Universities Scientific Fund, Grant/Award Numbers: 2018JQ01, 2018ZD01

Abstract

Concerning the mal-operation of distance protection in AC/DC hybrid system due to commutation failure in DC system caused by AC-side fault, a novel AC line distance protection scheme based on fault likeness factor is proposed. First, by analysing the conducting state of converter in different time intervals, the expression of feed-in current from DC system to AC system is derived. On this basis, combining AC-side fault component network, the fault location equation considering the impact of feed-in current from DC system is established. Thus, by solving the equation consisting of information at multiple time sections, the fault location is calculated. And then, according to the consistency between the calculated fault location and actual fault location, the fault likeness factor is constructed to distinguish between in-zone and out-of-zone faults. Finally, simulation tests in RT-LAB verify that, the proposed scheme can identify in-zone and out-of-zone faults fast and accurately in the case of commutation failure caused by different types of fault, strongly immune to fault resistance.

1 | INTRODUCTION

In recent years, with high voltage direct current (HVDC) transmission technology being widely applied in long-distance large-capacity power transmission, mal-operation of AC-side distance protection caused by commutation failure in DC system occurs ever more frequently, greatly endangering the safety and stability of power grid [1–7]. Therefore, fast and accurate isolation of AC-side fault is very important to guaranteeing the safe operation of AC/DC hybrid system.

Currently, AC line distance protection schemes mainly include distance protection based on traveling-wave distance measurement, distance protection based on power-frequency variables and time-domain distance protection. Distance protection based on traveling-wave distance measurement uses the refraction and reflection characteristic of traveling wave at impedance discontinuous points and locates the fault by calculating the time difference between forward traveling wave and backward traveling wave [8–10]. Due to the super high-speed operation characteristic of this method, it has become the focus of research on distance protection. However, in real system operation, fault or disturbance at any point of the grid will generate reflected waves, which may easily render the locating result inconsistent with the actual fault distance and cause distance protection to mal-operate. Distance protection

Nomenclature: $\triangle i_{mab}$, fault components of current difference between phase A and phase B at bus M; $\triangle i_{nab}$, fault component of current difference between phase A and phase B at bus N; $\triangle u_{mab}$, fault components of voltage difference between phase A and phase B at bus M; E_{ab}, voltage difference between phase A and phase B of AC system S_1; $f_{icom}(U)$, current that flows through AC filter and reactive power compensation device; i_{Ad}, i_{Bd}, i_{Cd}, i_{Ay}, i_{By}, i_{Cy}, currents on corresponding windings; i_d, DC current; i_f, current that flows through fault resistance; i_{f0}, zero-sequence current that flows through fault resistance; i_{mab}, current difference between phase A and phase B at bus M; i_{mabn}, current difference between phase A and phase B at bus M in normal operation state; i_{n0}, zero-sequence current at bus N; i_{na}, i_{nb}, i_{nc}, N-side three-phase currents; i_{nab}, current difference between phase A and phase B at bus N; i_{nabn}, current difference between phase A and phase B at bus N in normal operation state; k_d, transformation ratios of $Y/\triangle$ converter transformer; k_y, transformation ratios of Y/Y converter transformer; L_0, zero-sequence inductance of AC line M-N; L_d, inductance of smoothing reactor; L_1, positive-sequence inductance of AC line M-N; L_r, inductance of converter transformer converted to valve side; L_W, equivalent inductance of AC system S_1; L_{W0}, zero-sequence inductance of AC system S_1; R_0, zero-sequence resistance of AC line M-N; R_g, fault resistance; R_1, positive-sequence resistance of AC line M-N; R_W, equivalent resistance of AC system S_1; R_{W0}, zero-sequence resistance of AC system S_1; u_{m0}, zero-sequence voltage at bus M; u_{ma}, u_{mb}, u_{mc}, three-phase voltages at inverter-side converter bus; u_{mab}, voltage difference between phase A and phase B at bus M; x, fault location

based on power-frequency variables uses the power-frequency voltage at the beginning end of the protected line and the line power-frequency current information to form the protection criterion [11,12]. Compared to current protection and voltage protection, the protection range and sensitivity of distance protection based on power-frequency variables is less affected by the variation of operation mode of AC system. However, when DC system is integrated to AC system, AC-side fault may cause commutation failure in DC system, which will cause the equivalent feed-in current from DC system to AC system to change suddenly [13–15], thus the measured impedance will fluctuate, resulting in narrowed protection range or over-reach operation [16–18]. Time-domain distance protection is usually based on the assumption that the current distribution coefficients are constant, and uses parameter estimation method to calculate the fault distance [19]. This method is not affected by overload of line and system oscillation. However, when commutation failure occurs in DC system, due to non-linear time-varying fault characteristic of converter station and fast response of DC system controller, the equivalent impedance of DC system will keep changing, and the above assumption will not be true. Currently, research on AC line protection in the case of commutation failure is rare. Reference [17] uses the ratio of power-frequency current amplitude to current amplitude in normal operation state to construct the protection criterion. This method is applicable to commutation failure cases caused by AC-side fault. However, since the current amplitude ratio in fault state and current amplitude ratio in normal operation state are both close to 1, the reliability of this protection scheme is not adequate.

Concerning the inadaptability of distance protection based on power-frequency variables and time-domain distance protection to the integration of DC system to AC system, a novel AC line distance protection scheme based on fault likeness factor is proposed. First, by analysing the operating conditions of converter in different time intervals, the expression of feed-in current from DC system to AC system is derived. Second, according to AC-side fault component network, the fault location equation considering the impact of feed-in current from DC system is established. Thus, by solving the equation consisting of information at multiple time sections, the fault location is calculated. And then, the consistency between the calculated fault location and actual fault location is quantified as the fault likeness factor, based on which the protection criterion to identify in-zone and out-of-zone faults is constructed. Finally, simulation tests in RT-LAB verify the correctness and effectiveness of the proposed scheme. Compared with traditional methods, this paper builds the detailed model of AC/DC system that can reflect the conducting state of converter valves. Thus, the proposed scheme can identify in-zone and out-of-zone faults fast and accurately when commutation failure occurs in different fault cases (including fault at the outlet of AC line backside system). Besides, the proposed method is strongly immune to fault resistance, and is not affected by the variation of zero-sequence network of receiving-end AC system.

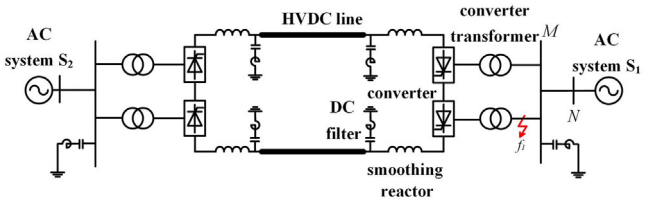

FIGURE 1 AC/DC hybrid system

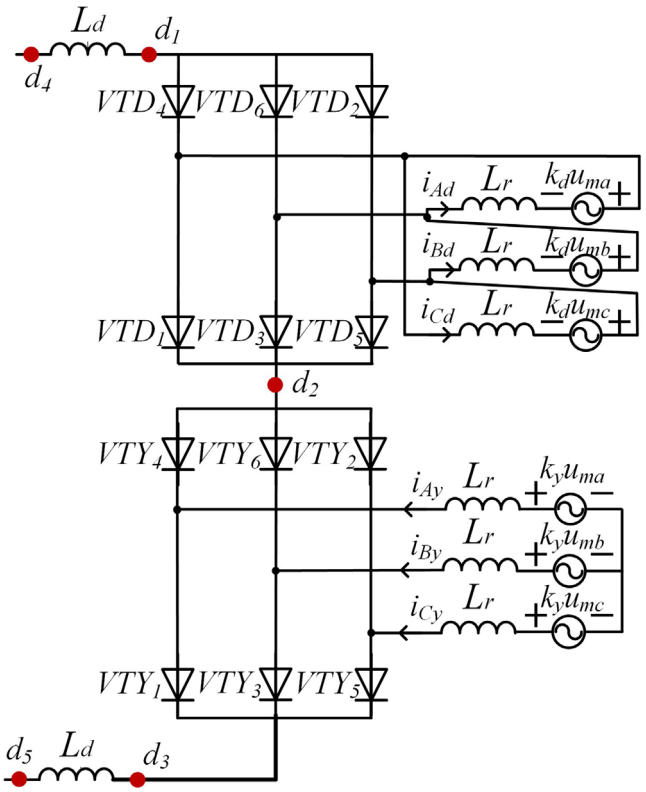

FIGURE 2 Wiring diagram of inverter-side 12-pulse converter

2 | EXPRESSION OF FEED-IN CURRENT FROM DC SYSTEM TO AC SYSTEM

Take the AC/DC hybrid system in Figure 1, for example. The wiring diagram of inverter-side 12-pulse converter is shown in Figure 2. When fault occurs on AC line, commutation failure may occur in inverter-side converter station due to AC-side fault, and inverter-side 12-pulse converter may operate in the following five conducting states.

a. Four valve arms of 12-pulse converter are conducted. For example, VTD_1 and VTD_2 of D-bridge converter are conducted; VTY_1 and VTY_2 of Y-bridge converter are conducted.
b. Five valve arms of 12-pulse converter are conducted. For example, VTD_1 and VTD_2 of D-bridge converter are con-

ducted; VTY_1, VTY_2 and VTY_3 of Y-bridge converter are conducted.

c. Six valve arms of 12-pulse converter are conducted. For example, VTD_1, VTD_4 and VTD_5 of D-bridge converter are conducted; VTY_1, VTY_4 and VTY_5 of Y-bridge converter are conducted.
d. Seven valve arms of 12-pulse converter are conducted. For example, VTD_1, VTD_4 and VTD_5 of D-bridge converter are conducted; VTY_1, VTY_4, VTY_5 and VTY_6 of Y-bridge converter are conducted.
e. Eight valve arms of 12-pulse converter are conducted. For example, VTD_1, VTD_4, VTD_5 and VTD_6 of D-bridge converter are conducted; VTY_1, VTY_4, VTY_5 and VTY_6 of Y-bridge converter are conducted.

When VTD_1 and VTD_2 of D-bridge converter, and VTY_1 and VTY_2 of Y-bridge converter are conducted, the following relationships can be obtained according to Figure 2:

$$i_d + i_{Cd} = i_{Bd} \tag{1}$$

$$i_{Bd} = i_{Ad} \tag{2}$$

$$u_d - u_{d1} = -k_d u_{ma} - k_d u_{mb} + 2L_r \frac{di_{Bd}}{dt} \tag{3}$$

$$u_d - u_{d1} = k_d u_{mc} - L_r \frac{di_{Cd}}{dt} \tag{4}$$

$$i_{Ay} = -i_{Cy} = i_d \tag{5}$$

$$i_{By} = 0 \tag{6}$$

$$u_{d1} - u_{d2} = k_y(u_{mc} - u_{ma}) + 2L_r \frac{di_d}{dt} \tag{7}$$

$$u_{drec} = u_d + L_d \frac{di_d}{dt} \tag{8}$$

$$u_{drec2} = u_{d2} - L_d \frac{di_d}{dt}, \tag{9}$$

where u_{ma}, u_{mb} and u_{mc} are three-phase voltages at inverter-side converter bus. u_d, u_{d1}, u_{d2}, u_{drec} and u_{drec2} are, respectively, the voltages at d_1, d_2, d_3, d_4 and d_5 in Figure 2. i_{Ad}, i_{Bd}, i_{Cd}, i_{Ay}, i_{By} and i_{Cy} are the currents on the corresponding windings. i_d is DC current. k_y and k_d are the transformation ratios of Y/Y converter transformer and Y/△ converter transformer. L_r is the inductance of converter transformer converted to the valve side. L_d is the inductance of smoothing reactor.

According to (1)–(4), the following equations can be obtained:

$$\begin{cases} k_d(u_{ma} + u_{mb} + u_{mc}) = 3L_r \frac{di_{Ad}}{dt} - L_r \frac{di_d}{dt} \\ k_d(u_{ma} + u_{mb} + u_{mc}) = 3L_r \frac{di_{Bd}}{dt} - L_r \frac{di_d}{dt} \\ k_d(u_{ma} + u_{mb} + u_{mc}) = 3L_r \frac{di_{Cd}}{dt} + 2L_r \frac{di_d}{dt} \end{cases}. \tag{10}$$

Combining (2), (3), (4) and (7) yields:

$$\begin{cases} u_d - u_{d2} = -(k_d + k_y)u_{ma} - k_d u_{mb} + k_y u_{mc} \\ \qquad + 2L_r \frac{di_{Ad}}{dt} + 2L_r \frac{di_d}{dt} \\ u_d - u_{d2} = -(k_d + k_y)u_{ma} - k_d u_{mb} + k_y u_{mc} \\ \qquad + 2L_r \frac{di_{Bd}}{dt} + 2L_r \frac{di_d}{dt} \\ u_d - u_{d2} = -k_y u_{ma} + (k_d + k_y)u_{mc} \\ \qquad - L_r \frac{di_{Cd}}{dt} + 2L_r \frac{di_d}{dt} \end{cases}. \tag{11}$$

According to (8)–(11), the difference between voltages at d_4 and d_5 has the following relationships with the current on valve-side winding of Y/△ converter transformer:

$$\begin{cases} u_{drec} - u_{drec2} = -(3k_d + k_y + \frac{2L_d}{L_r}k_d)u_{ma} - (3k_d + \frac{2L_d}{L_r}k_d)u_{mb} \\ \qquad + (k_y - 2k_d - \frac{2L_d}{L_r}k_d)u_{mc} + (8L_r + 6L_d)\frac{di_{Ad}}{dt} \\ u_{drec} - u_{drec2} = -(3k_d + k_y + \frac{2L_d}{L_r}k_d)u_{ma} - (3k_d + \frac{2L_d}{L_r}k_d)u_{mb} \\ \qquad + (k_y - 2k_d - \frac{2L_d}{L_r}k_d)u_{mc} + (8L_r + 6L_d)\frac{di_{Bd}}{dt} \\ u_{drec} - u_{drec2} = (\frac{L_d}{L_r}k_d + k_d - k_y)u_{ma} + (k_d + \frac{L_d}{L_r}k_d)u_{mb} \\ \qquad + (2k_d + k_y + \frac{L_d}{L_r}k_d)u_{mc} - (4L_r + 3L_d)\frac{di_{Cd}}{dt} \end{cases}. \tag{12}$$

And according to (5), (6), (10) and (12), the difference between voltages at d_4 and d_5 has the following relationships with the current on valve-side winding of Y/Y converter transformer:

$$\begin{cases} u_{drec} - u_{drec2} = -(\frac{1}{3}k_d + k_y)u_{ma} - \frac{1}{3}k_d u_{mb} \\ \qquad + (k_y + \frac{2}{3}k_d)u_{mc} + (\frac{8}{3}L_r + 2L_d)\frac{di_{Ay}}{dt} \\ 0 = \frac{di_{By}}{dt} \\ u_{drec} - u_{drec2} = -(\frac{1}{3}k_d + k_y)u_{ma} - \frac{1}{3}k_d u_{mb} \\ \qquad + (k_y + \frac{2}{3}k_d)u_{mc} - (\frac{8}{3}L_r + 2L_d)\frac{di_{Cy}}{dt} \end{cases}. \tag{13}$$

Equations (12) and (13) can be written in the form of matrices, as shown in (14) and (15):

$$D_{d4} = A_{d4}U + \frac{dI_d}{dt} \tag{14}$$

$$D_{y4} = A_{y4}U + \frac{dI_y}{dt}, \tag{15}$$

where I_d, I_y, U, D_{d4}, D_{y4}, A_{d4} and A_{y4} are, respectively,

$$I_d = \begin{bmatrix} i_{Ad} \\ i_{Bd} \\ i_{Cd} \end{bmatrix}, I_y = \begin{bmatrix} i_{Ay} \\ i_{By} \\ i_{Cy} \end{bmatrix}, U = \begin{bmatrix} u_{ma} \\ u_{mb} \\ u_{mc} \end{bmatrix}$$

$$D_{d4}=\begin{bmatrix}\frac{u_{drec}-u_{drec2}}{8L_r+6L_d}\\ \frac{u_{drec}-u_{drec2}}{8L_r+6L_d}\\ \frac{u_{drec2}-u_{drec}}{4L_r+3L_d}\end{bmatrix},\ D_{y4}=\begin{bmatrix}\frac{3u_{drec}-3u_{drec2}}{8L_r+6L_d}\\ 0\\ \frac{3u_{drec2}-3u_{drec}}{8L_r+6L_d}\end{bmatrix}$$

$$A_{d4}=\begin{bmatrix}\frac{-3k_dL_r-k_yL_r-2L_dk_d}{8L_r^2+6L_dL_r} & \frac{-3k_dL_r-2L_dk_d}{8L_r^2+6L_dL_r} & \frac{k_yL_r-2k_dL_r-2L_dk_d}{8L_r^2+6L_dL_r}\\ \frac{-3k_dL_r-k_yL_r-2L_dk_d}{8L_r^2+6L_dL_r} & \frac{-3k_dL_r-2L_dk_d}{8L_r^2+6L_dL_r} & \frac{k_yL_r-2k_dL_r-2L_dk_d}{8L_r^2+6L_dL_r}\\ \frac{L_dk_d+k_dL_r-k_yL_r}{-4L_r^2-3L_dL_r} & \frac{k_dL_r+L_dk_d}{-4L_r^2-3L_dL_r} & \frac{L_dk_d+2k_dL_r+k_yL_r}{-4L_r^2-3L_dL_r}\end{bmatrix}$$

$$A_{y4}=\begin{bmatrix}\frac{-k_d-3k_y}{8L_r+6L_d} & \frac{-k_d}{8L_r+6L_d} & \frac{3k_y+2k_d}{8L_r+6L_d}\\ 0 & 0 & 0\\ \frac{k_d+3k_y}{8L_r+6L_d} & \frac{k_d}{8L_r+6L_d} & \frac{-3k_y-2k_d}{8L_r+6L_d}\end{bmatrix}.$$

Combine (14) and (15), so that the feed-in current from DC system to AC system can be calculated:

$$I=\int[(K_dA_{d4}+K_yA_{y4})U-K_dD_{d4}-K_yD_{y4}]dt+f_{icom}(U), \tag{16}$$

where $f_{icom}(U)$ is the current that flows through AC filter and reactive power compensation device. When the parameters of AC filter and reactive power compensation device are fixed, $f_{icom}(U)$ is the function of converter bus voltage U. Matrices I, K_y and K_d are, respectively,

$$I=\begin{bmatrix}i_{ma}\\ i_{mb}\\ i_{mc}\end{bmatrix},\ K_y=\begin{bmatrix}k_y & 0 & 0\\ 0 & k_y & 0\\ 0 & 0 & k_y\end{bmatrix},\ K_d=\begin{bmatrix}k_d & 0 & 0\\ 0 & k_d & 0\\ 0 & 0 & k_d\end{bmatrix}.$$

When another four valve arms of 12-pulse converter are conducted, or five/six/seven/eight valve arms of 12-pulse converter are conducted, similar derivation process can be applied. By combining the conducting states of converter valves and the wiring diagram in Figure 2, relationships similar to (1)–(7) can be established, and the expression of feed-in current from DC system to AC system in the same form as (16) can be obtained.

3 | EQUATIONS OF FAULT LOCATION CORRESPONDING TO DIFFERENT TYPES OF FAULT ON AC LINE

The protection criterion of traditional distance protection is composed of AC-side fault information and does not consider the impact of feed-in current from DC system on the measured impedance, thus when AC-side fault results in commutation failure, distance protection may mal-operate or refuse to operate. To solve this problem, the feed-in current from DC system is introduced to AC-side faulty network, thus equations of fault location under different fault types are constructed.

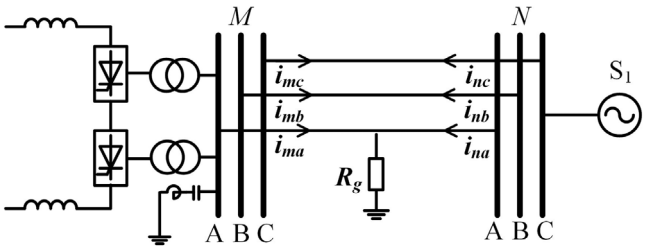

FIGURE 3 Diagram of single-phase-to-ground fault

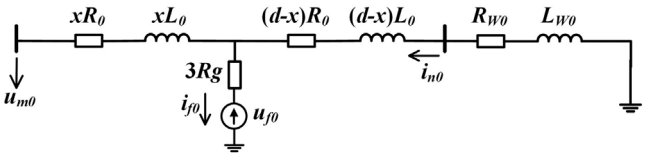

FIGURE 4 AC-side zero-sequence fault component network

3.1 | Fault location equation in the case of single-phase-to-ground fault

When phase-A-to-ground fault occurs at location x on AC line M-N with the fault resistance being R_g, the fault system is shown in Figure 3, where i_{na}, i_{nb} and i_{nc} are N-side three-phase currents. The AC-side zero-sequence fault component network is shown in Figure 4, where $d=1$. R_{W0} and L_{W0} are zero-sequence resistance and inductance of AC system S_1. R_0 and L_0 are zero-sequence resistance and inductance of AC line M-N. i_{f0} is the zero-sequence current that flows through the fault resistance. u_{m0} and i_{n0} are, respectively, zero-sequence voltage at bus M and zero-sequence current at bus N.

According to Figure 3, the voltage of phase A at the fault point can be written as

$$u_{fa}=u_{ma}-xR_l(i_{ma}+3k_Ri_{m0})-xL_l\frac{d(i_{ma}+3k_Li_{m0})}{dt}, \tag{17}$$

where R_l and L_l are, respectively, positive-sequence resistance and positive-sequence inductance of AC line M-N.

In (17), the expressions of i_{m0}, k_R and k_L are, respectively,

$$i_{m0}=\frac{i_{ma}+i_{mb}+i_{mc}}{3} \tag{18}$$

$$k_R=\frac{R_0-R_l}{3R_l} \tag{19}$$

$$k_L=\frac{L_0-L_l}{3L_l}. \tag{20}$$

According to Figure 3, the following relationships exist between M-side three-phase currents and N-side three-phase

currents:

$$\begin{cases} i_{ma} + i_{na} = i_f \; i_{mb} = -i_{nb} \\ i_{mc} = -i_{nc} \end{cases}, \tag{21}$$

where i_f is the current that flows through the fault resistance.

According to (18) and (21), the voltage of phase A at the fault point is

$$u_{fa} = 3(i_{m0} + i_{n0})R_g. \tag{22}$$

Apply (22) to (17) so that

$$\begin{aligned} &3(i_{m0} + i_{n0})R_g \\ &= u_{ma} - xR_l(i_{ma} + 3k_R i_{m0}) - xL_l \frac{d(i_{ma}+3k_L i_{m0})}{dt}. \end{aligned} \tag{23}$$

According to Figure 4, the voltage calculated from bus M towards the fault point is equal to the voltage calculated from bus N towards the fault point, thus

$$\begin{aligned} &u_{m0} - xR_0 i_{m0} - xL_0 \frac{di_{m0}}{dt} \\ &= -[(d-x)R_0 + R_{W0}]i_{n0} - [(d-x)L_0 + L_{W0}]\frac{di_{n0}}{dt}. \end{aligned} \tag{24}$$

Combine (23) and (24) so that

$$p_1 + p_2 R_g + p_3 x + p_4 x^2 = 0, \tag{25}$$

where the expressions of p_1, p_2, p_3 and p_4 are

$$\begin{cases} p_1 = dL_0 \frac{du_{ma}}{dt} + L_{W0}\frac{du_{ma}}{dt} + dR_0 u_{ma} + R_{W0}u_{ma} \\ p_2 = 3(-dL_0\frac{di_{m0}}{dt} - L_{W0}\frac{di_{m0}}{dt} - dR_0 i_{m0} - R_{W0}i_{m0} + u_{m0}) \\ p_4 = L_0 L_l \frac{d^2 i_{ma}}{dt^2} + 3k_L L_0 L_l \frac{d^2 i_{m0}}{dt^2} + L_l R_0 \frac{di_{ma}}{dt} \\ \quad + 3k_L L_l R_0 \frac{di_{m0}}{dt} + L_0 L_l \frac{di_{ma}}{dt} \\ \quad + 3k_R L_0 R_l \frac{di_{m0}}{dt} + R_0 R_l i_{ma} + 3k_R R_0 R_l i_{m0} \\ p_3 = -L_0 \frac{du_{ma}}{dt} - dL_0 L_l \frac{d^2 i_{ma}}{dt^2} - 3dk_L L_0 L_l \frac{d^2 i_{m0}}{dt^2} \\ \quad - L_{W0}L_l \frac{d^2 i_{ma}}{dt^2} - 3k_L L_{W0} L_l \frac{d^2 i_{m0}}{dt^2} - dL_l R_0 \frac{di_{ma}}{dt} \\ \quad - 3dk_L L_l R_0 \frac{di_{m0}}{dt} - dL_0 R_l \frac{di_{ma}}{dt} - 3dk_R L_0 R_l \frac{di_{m0}}{dt} \\ \quad - L_{W0}R_l \frac{di_{ma}}{dt} - 3k_R L_{W0} R_l \frac{di_{m0}}{dt} - dR_0 R_l i_{ma} \\ \quad - 3k_R dR_0 R_l i_{m0} - L_l R_{W0} \frac{di_{ma}}{dt} - 3k_L L_l R_{W0} \frac{di_{m0}}{dt} \\ \quad - R_l R_{W0} i_{ma} - 3k_R R_l R_{W0} i_{m0} - R_0 u_{ma} \end{cases}. \tag{26}$$

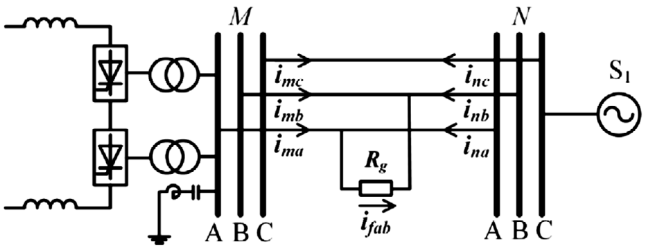

FIGURE 5 Diagram of phase-to-phase fault

3.2 | Fault location equation in the case of phase-to-phase fault

When phase-A-to-phase-B fault occurs at location x on AC line M-N with the fault resistance being R_g, the fault system is shown in Figure 5, where i_{fab} is the current that flows through the fault resistance.

According to Figure 5, the voltages of phase A and phase B at the fault point are, respectively,

$$\begin{cases} u_{fa} = u_{ma} - xR_l(i_{ma} + 3k_R i_{m0}) - xL_l \frac{d(i_{ma}+3k_R i_{m0})}{dt} \\ u_{fb} = u_{mb} - xR_l(i_{mb} + 3k_R i_{m0}) - xL_l \frac{d(i_{mb}+3k_R i_{m0})}{dt} \end{cases}. \tag{27}$$

Thus, the voltage difference between phase A and phase B at the fault point is

$$u_{fab} = u_{mab} - xR_l i_{mab} - xL_l \frac{di_{mab}}{dt}, \tag{28}$$

where u_{mab} and i_{mab} are, respectively, the voltage difference and current difference between phase A and phase B at bus M.

According to Figure 5,

$$\begin{cases} u_{fab} = (i_{ma} + i_{na})R_g \\ -u_{fab} = (i_{mb} + i_{nb})R_g \end{cases}. \tag{29}$$

Thus,

$$2u_{fab} = (i_{mab} + i_{nab})R_g, \tag{30}$$

where i_{nab} is the current difference between phase A and phase B at bus N.

Apply (30) to (28) so that

$$(i_{mab} + i_{nab})\frac{R_g}{2} = u_{mab} - xR_l i_{mab} - xL_l \frac{di_{mab}}{dt}. \tag{31}$$

According to (31), the fault state network of phase-to-phase short circuit fault can be obtained, as shown in Figure 6(a), while the fault component network of phase-to-phase short circuit fault is shown in Figure 6(b).

In Figure 6(a), E_{ab} is the voltage difference between phase A and phase B of AC system S_1. In Figure 6(b), $\triangle u_{mab}$ and $\triangle i_{mab}$ are, respectively, the fault components of voltage difference and current difference between phase A and phase B at bus M. $\triangle i_{nab}$ is the fault component of current difference between phase A and phase B at bus N. R_W and L_W are the equivalent resistance and inductance of AC system S_1.

According to Figure 6(b), the voltage calculated from bus M towards the fault point is equal to the voltage calculated from bus N towards the fault point, thus,

$$\begin{aligned}&\Delta u_{mab} - xR_l\Delta i_{mab} - xL_l\Delta\frac{di_{mab}}{dt}\\&\quad= -[R_W + (d-x)R_l]\Delta i_{nab} - [L_W + (d-x)L_l]\Delta\frac{di_{nab}}{dt}.\end{aligned} \tag{32}$$

According to the superposition theorem,

$$\begin{cases} i_{mab} = i_{mabn} + \Delta i_{mab} \\ i_{nab} = i_{nabn} + \Delta i_{nab} \end{cases}, \tag{33}$$

where i_{mabn} and i_{nabn} are, respectively, the current difference between phase A and phase B at bus M and the current difference between phase A and phase B at bus N in normal operation state.

According to (33),

$$i_{mab} + i_{nab} = \Delta i_{mab} + \Delta i_{nab}. \tag{34}$$

Apply (34) to (31) so that

$$(\Delta i_{mab} + \Delta i_{nab})\frac{R_g}{2} = u_{mab} - xR_l i_{mab} - xL_l\frac{di_{mab}}{dt}. \tag{35}$$

Combining (32) and (35) yields

$$p_5 + p_6R_g + p_7x + p_8x^2 = 0, \tag{36}$$

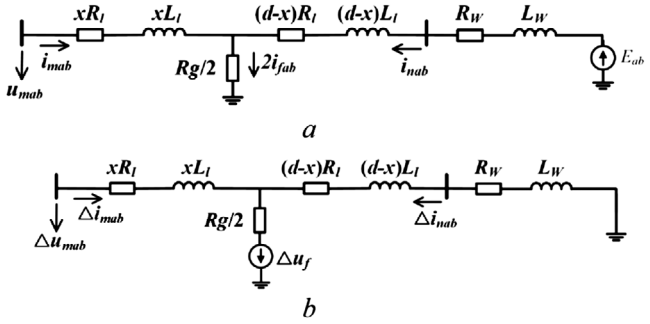

FIGURE 6 Fault networks of phase-to-phase short circuit fault (a) Fault state network of phase-to-phase short circuit fault, (b) Fault component network of phase-to-phase short circuit fault

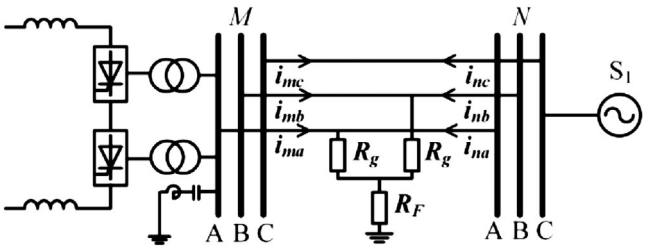

FIGURE 7 Diagram of phase-to-phase grounding fault

where the expressions of p_5, p_6, p_7 and p_8 are

$$\begin{cases} p_5 = 2dL_l\frac{du_{mab}}{dt} + 2L_W\frac{du_{mab}}{dt} + 2dR_l u_{mab} + 2R_W u_{mab} \\ p_6 = \Delta u_{mab} - dL_l\Delta\frac{di_{mab}}{dt} - L_W\Delta\frac{di_{mab}}{dt} \\ \qquad - d\Delta i_{mab}R_l - \Delta i_{mab}R_W \\ p_7 = -2L_l\frac{du_{mab}}{dt} - 2dL_l^2\frac{d^2i_{mab}}{dt^2} \\ \qquad - 2L_WL_l\frac{d^2i_{mab}}{dt^2} - 4dL_lR_l\frac{di_{mab}}{dt} \\ \qquad - 2L_WR_l\frac{di_{mab}}{dt} - 2dR_l^2i_{mab} \\ \qquad - 2L_lR_W\frac{di_{mab}}{dt} - 2R_lR_Wi_{mab} - 2R_lu_{mab} \\ p_8 = 2L_l^2\frac{d^2i_{mab}}{dt^2} + 4L_lR_l\frac{di_{mab}}{dt} + 2R_l^2i_{mab} \end{cases}. \tag{37}$$

3.3 | Fault location equation in the case of other fault types

3.3.1 | Phase-to-phase grounding fault

When phase-AB-to-ground fault occurs at location x on AC line M-N, the fault system is shown in Figure 7, where the voltage difference between phase A and phase B at the fault point is shown in (28).

According to Figure 7,

$$\begin{cases} u_{fa} = (i_{ma} + i_{na})R_g + (i_{ma} + i_{na} + i_{mb} + i_{nb})R_F \\ u_{fb} = (i_{mb} + i_{nb})R_g + (i_{ma} + i_{na} + i_{mb} + i_{nb})R_F \end{cases}. \tag{38}$$

According to (38),

$$u_{fab} = (i_{mab} + i_{nab})R_g. \tag{39}$$

Combine (28) and (39) so that

$$(i_{mab} + i_{nab})R_g = u_{mab} - xR_l i_{mab} - xL_l\frac{di_{mab}}{dt}. \tag{40}$$

Comparing (35) and (40), it can be seen that the circuit of phase-to-phase grounding fault can be decomposed into fault networks similar to those in Figure 6, and by applying the

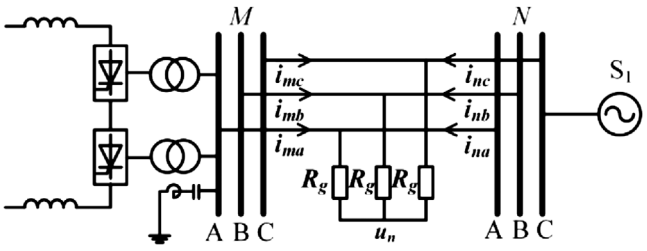

FIGURE 8 Diagram of three-phase short circuit fault

derivation process similar to that of phase-to-phase fault, the fault location equation in the case of phase-to-phase grounding fault can be obtained:

$$p_5 + 2p_6R_g + p_7x + p_8x^2 = 0. \tag{41}$$

3.3.2 | Three-phase short circuit fault

When three-phase short circuit fault occurs at location x on AC line M-N, the fault system is shown in Figure 8.

According to Figure 8,

$$\begin{cases} u_{fa} = (i_{ma} + i_{na})R_g + u_n \\ u_{fb} = (i_{mb} + i_{nb})R_g + u_n \end{cases}, \tag{42}$$

where u_n is the voltage at the corresponding point in Figure 8.

According to (42),

$$u_{fab} = (i_{mab} + i_{nab})R_g. \tag{43}$$

Comparing (39) and (43), it can be seen that, when three-phase short circuit fault occurs, the expression of voltage difference between any two phases at the fault point is the same as that in the case of phase-to-phase grounding fault. Therefore, by applying the data of any two phases to the fault location equation of phase-to-phase grounding fault, the fault location of three-phase short circuit fault can be calculated.

It can be seen from (25), (36) and (41) that, when different types of fault occur on AC line, the unified expression of fault location equation is

$$p_c + p_{rg}R_g + p_xx + p_{x2}x^2 = 0. \tag{44}$$

In (44), when single phase grounding fault occurs, $p_c = p_1$, $p_{rg} = p_2$, $p_x = p_3$, $p_{x2} = p_4$; when phase-to-phase fault occurs, $p_c = p_5$, $p_{rg} = p_6$, $p_x = p_7$, $p_{x2} = p_8$; when phase-to-phase grounding fault or three-phase short circuit fault occurs, $p_c = p_5$, $p_{rg} = 2p_6$, $p_x = p_7$, $p_{x2} = p_8$.

According to the above analysis, only the fault location and fault resistance are unknown in fault location equation. After fault occurs, with the fault instant as the starting point, fault data in the time window of 10 ms are collected. For any two sampling points in the 10 ms, two binary quadratic equations are constructed according to (44). Then Newton iteration method is used to calculate the fault location. Since there are more than two sampling points, the redundant information is used for nonlinear least square optimisation of fault location, so that the calculation error of fault location can be reduced. The optimisation process applies Gauss-Newton method, the detailed steps of which are shown below.

Step 1: Set initial values of fault resistance and fault location $R_g(0)$ and $x(0)$. The initial value of fault resistance can be set as 300Ω in the case of single phase grounding fault, and 100Ω in the case of other fault types. The initial value of fault location can be set as the whole line length.

Step 2: For the kth iteration, calculate Jacobian matrix J.

Step 3: For the kth iteration, calculate matrix $H = J^TJ$.

Step 4: For the kth iteration, calculate matrix $B = -J^Tf$, where $f = p_c(i) + p_{rg}(i)R_g + p_x(i)x + p_{x2}(i)x^2$.

Step 5: For the kth iteration, calculate $\triangle X_k = H^{-1}B$.

Step 6: If $\triangle X_k$ is small enough or the number of iterations reaches the maximum value, stop iteration; otherwise, update $X_{k+1} = \triangle X_k + X_k$.

Step 7: According to the premise of derivation process in Section 3, fault distance x satisfies $0 \le x \le d$. Thus if the calculated fault distance x exceeds the whole line length d, the fault distance is taken as the whole line length; if the calculated fault distance x is below 0, the fault distance is taken as 0.

3.4 | AC line distance protection scheme based on fault likeness factor

Suppose four valve arms of inverter-side converter are conducted, currents i_{ma}, i_{mb} and i_{mc} in such conducting state are calculated according to (16).

When fault occurs in the DC system on the backside of bus M, according to the fault location, it may be fault in D-bridge converter, Y-bridge converter or AC filter. For D-bridge converter fault, (1) and (2) are not satisfied; for Y-bridge converter fault, (5) and (6) are not satisfied; for AC filter fault, the currents calculated according to the normal model of AC filter are inconsistent with the actual currents that flow through AC filter. Since (16) is derived according to (1), (2), (5), (6) and the normal model of AC filter, in the above fault cases, currents i_{ma}, i_{mb} and i_{mc} calculated according to (16) will deviate from the actual values. Consider that (44) is based on the actual values of currents i_{ma}, i_{mb} and i_{mc}, in the above fault cases (44) is not satisfied, that is,

$$p_c + p_{rg}R_g + p_xx + p_{x2}x^2 \neq 0. \tag{45}$$

When in-zone fault occurs on AC line M-N, there is not fault point in DC system, thus (1), (2), (5), (6) are satisfied, and currents i_{ma}, i_{mb} and i_{mc} calculated according to (16) are consistent with the actual values. Also, since (44) is based on the actual values of currents i_{ma}, i_{mb} and i_{mc}, in this fault case (44) is

satisfied, that is,

$$p_c + p_{rg}R_g + p_x x + p_{x2}x^2 = 0. \tag{46}$$

When fault occurs on the downstream line of AC line M-N, the calculated fault distance x exceeds the whole length of AC line M-N. In this case, according to Step 7 of non-linear least square optimisation in the revised paper, the whole length of AC line M-N is taken as the calculated fault distance. Consider that (44) is based on the actual fault distance, in this fault case (44) is not satisfied, that is,

$$p_c + p_{rg}R_g + p_x x + p_{x2}x^2 \neq 0. \tag{47}$$

According to the above analysis, when in-zone fault occurs on AC line M-N, the fault location calculated according to (44) is consistent with the actual fault location. But when fault occurs on the subordinate lines of line M-N or in the DC system on the backside of bus M, (44) is not be satisfied, and the fault location calculated according to (44) will deviate from the actual fault location. In order to quantify the consistency between the calculated fault location and actual fault location, the fault likeness factor is defined. The fault likeness factor is constructed with the reciprocal of the left term in (45)–(47), that is,

$$S_{\mathrm{HVDC}} = \sum_{i=1}^{n} \frac{1}{\left| p_c(i) + p_{rg}(i)R_g + p_x(i)x + p_{x2}(i)x^2 \right|}, \tag{48}$$

where n is the number of sampling points in 10 ms. $p_c(i)$, $p_{rg}(i)$, $p_x(i)$ and $p_{x2}(i)$ are, respectively, the values of p_c, p_{rg}, p_x and p_{x2} calculated according to the fault data of the ith sampling point.

According to the above analysis, the proposed AC line distance protection scheme based on fault likeness factor can be realised in the following steps.

Step 1: Use differential current transformer to monitor the turn-on and turn-off states of converter valves and determine the conducting state of converter, and calculate the feed-in current from DC system to AC system.

Step 2: Apply the sampling value of voltage at the relaying point of line M-N and the value of feed-in current obtained in Step 1 to the fault location equation to calculate the fault location and fault resistance.

Step 3: Apply the calculated fault location and fault resistance to (48) to calculate fault likeness factor S_{HVDC}.

Step 4: If the fault likeness factor exceeds the threshold value, it is identified that the fault is in the protection zone of line M-N; otherwise, the fault is outside the protection zone.

Consider that in calculation process, the fault likeness factor will be affected by measuring errors, the threshold value is set to be 5.

3.5 | The effect of changes in the R_{W0} and L_{W0} parameters in the performance of the proposed method

R_{W0} and L_{W0} are zero-sequence impedance parameters of receiving-end AC system, which are mainly determined by zero-sequence impedances of transmission line and neutral grounding transformer. Thus only when the transmission line or transformer is switched on/off, system zero-sequence impedance will change. Consider that the time interval between two switchings of line or transformer is much longer than the operation time of protection, during the identification of fault location, R_{W0} and L_{W0} can be approximated as constants.

Combining (25) and (26) yields:

$$\begin{aligned} &p_{i1} + p_{i2}L_{W0} + p_{i3}R_{W0} + p_{i4}R_g + p_{i5}L_{W0}R_g \\ &\quad + p_{i6}R_{W0}R_g + p_{i7}x + p_{i8}L_{W0}x + p_{i9}R_{W0}x + p_{i10}x^2 = 0, \end{aligned} \tag{49}$$

where p_{i1}, p_{i2}, p_{i3}, p_{i4}, p_{i5}, p_{i6}, p_{i7}, p_{i8}, p_{i9} and p_{i10} are, respectively,

$$\begin{cases} p_{i1} = dL_0\frac{du_{ma}}{dt} + dR_0u_{ma},\ p_{i2} = \frac{du_{ma}}{dt},\ p_{i3} = u_{ma} \\ p_{i4} = 3(-dL_0\frac{di_{m0}}{dt} - dR_0i_{m0} + u_{m0}),\ p_{i5} = -3\frac{di_{m0}}{dt},\ p_{i6} = -3i_{m0} \\ p_{i7} = -L_0\frac{du_{ma}}{dt} - dL_0L_l\frac{d^2i_{ma}}{dt^2} - 3dk_LL_0L_l\frac{d^2i_{m0}}{dt^2} \\ \qquad - dL_lR_0\frac{di_{ma}}{dt} - 3dk_LL_lR_0\frac{di_{m0}}{dt} - dL_0R_l\frac{di_{ma}}{dt} \\ \qquad - 3dk_RL_0R_l\frac{di_{m0}}{dt} - dR_0R_li_{ma} - 3k_RdR_0R_li_{m0} - R_0u_{ma} \\ p_{i8} = -L_l\frac{d^2i_{ma}}{dt^2} - 3k_LL_l\frac{d^2i_{m0}}{dt^2} - R_l\frac{di_{ma}}{dt} - 3k_RR_l\frac{di_{m0}}{dt} \\ p_{i9} = -L_l\frac{di_{ma}}{dt} - 3k_LL_l\frac{di_{m0}}{dt} - R_li_{ma} - 3k_RR_li_{m0} \\ p_{i10} = L_0L_l\frac{d^2i_{ma}}{dt^2} + 3k_LL_0L_l\frac{d^2i_{m0}}{dt^2} + L_lR_0\frac{di_{ma}}{dt} \\ \qquad + 3k_LL_lR_0\frac{di_{m0}}{dt} + L_0L_l\frac{di_{ma}}{dt} \\ \qquad + 3k_RL_0R_l\frac{di_{m0}}{dt} + R_0R_li_{ma} + 3k_RR_0R_li_{m0} \end{cases} \tag{50}$$

After fault occurs, with the fault instant as the starting point, fault data in the time window of 10 ms are collected. For any two sampling points in the 10 ms, combining (49) and (50) yields:

$$\begin{cases} p_{i1}(j) + p_{i2}(j)L_{W0} + p_{i3}(j)R_{W0} \\ \quad + p_{i4}(j)R_g + p_{i5}(j)L_{W0}R_g \\ \quad + p_{i6}(j)R_{W0}R_g + p_{i7}(j)x \\ \quad + p_{i8}(j)L_{W0}x + p_{i9}(j)R_{W0}x + p_{i10}(j)x^2 = 0 \\ p_{i1}(j+1) + p_{i2}(j+1)L_{W0} + p_{i3}(j+1)R_{W0} \\ \quad + p_{i4}(j+1)R_g + p_{i5}(j+1)L_{W0}R_g \\ \quad + p_{i6}(j+1)R_{W0}R_g + p_{i7}(j+1)x \\ \quad + p_{i8}(j+1)L_{W0}x + p_{i9}(j+1)R_{W0}x + p_{i10}(j+1)x^2 = 0 \end{cases} \tag{51}$$

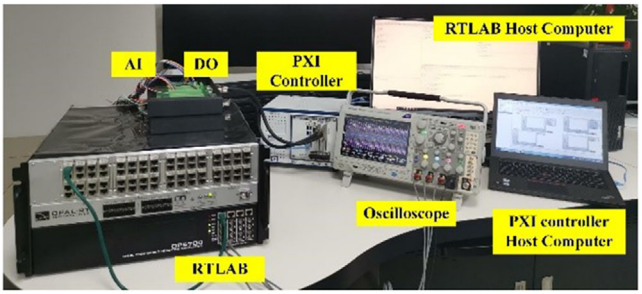

FIGURE 9 RT-LAB test platform

In (51), eliminating R_{W0} and L_{W0} yields:

$$\begin{aligned}&(b_1 - a_1)[p_{i4}(j)R_g + p_{i7}(j)x + p_{i10}(j)x^2 + p_{i1}(j)]\\&\quad + [p_{i3}(j) + p_{i6}(j)R_g + p_{i9}(j)x](a_2 - b_2)\\&\quad - [p_{i2}(j) + p_{i8}(j)x + p_{i5}(j)R_g][a_1 b_1 (a_3 - b_3)] = 0,\end{aligned} \tag{52}$$

where a_1, a_2, a_3, b_1, b_2 and b_3 are, respectively,

$$\begin{cases} a_1 = \dfrac{p_{i3}(j)+p_{i6}(j)R_g+p_{i9}(j)x}{p_{i2}(j)+p_{i8}(j)x+p_{i5}(j)R_g} \\ a_2 = \dfrac{p_{i1}(j)+p_{i4}(j)R_g+p_{i7}(j)x+p_{i10}(j)x^2}{[p_{i2}(j)+p_{i8}(j)x+p_{i5}(j)R_g]} \\ a_3 = \dfrac{p_{i1}(j)+p_{i4}(j)R_g+p_{i7}(j)x+p_{i10}(j)x^2}{[p_{i3}(j)+p_{i6}(j)R_g+p_{i9}(j)x]} \\ b_1 = \dfrac{p_{i3}(j+1)+p_{i6}(j+1)R_g+p_{i9}(j+1)x}{p_{i2}(j+1)+p_{i8}(j+1)x+p_{i5}(j+1)R_g} \\ b_2 = \dfrac{p_{i1}(j+1)+p_{i4}(j+1)R_g+p_{i7}(j+1)x+p_{i10}(j+1)x^2}{[p_{i2}(j+1)+p_{i8}(j+1)x+p_{i5}(j+1)R_g]} \\ b_3 = \dfrac{p_{i1}(j+1)+p_{i4}(j+1)R_g+p_{i7}(j+1)x+p_{i10}(j+1)x^2}{[p_{i3}(j+1)+p_{i6}(j+1)R_g+p_{i9}(j+1)x]} \end{cases}. \tag{53}$$

In the equation of fault location shown in (52), fault resistance and fault location are the only unknown numbers. Then, another two sampling points are taken to establish two binary quadratic equations similar to (52), and Newton iteration method is used to calculate the fault location. Since the equations do not contain R_{W0} or L_{W0}, the impact of R_{W0} and L_{W0} on the calculated fault location can be neglected.

4 | SIMULATION VERIFICATION

4.1 | Test system

Hardware-in-loop tests are conducted to verify the effectiveness of the proposed method. The hardware-in-loop platform consists of RT-LAB and CPU controller based on PXI protocol, as shown in Figure 9, where the main circuit is AC/DC hybrid system shown in Figure 1 operating in RT-LAB, and the control algorithm operates in CPU controller. The main parameters of AC/DC hybrid system are shown in Table 1. The fault is set to occur at $t = 0$.

TABLE 1 Main parameters of AC/DC hybrid system

Parameter	Value
Frequency	50 Hz
Capacity of inverter-side converter transformer	598 MVA
Transformation ratio of inverter-side converter transformer	331.2 kV/200.6 kV
Rated voltage of inverter-side converter bus	330 kV
Impedance percentage of inverter-side converter transformer	16%
Inductance of smoothing reactor	500 mH
Length of AC line M-N	80 km
Positive-sequence resistance of AC line M-N	0.0216Ω/km
Positive-sequence reactance of AC line M-N	0.2750Ω/km
Zero-sequence resistance of AC line M-N	0.1672Ω/km
Zero-sequence reactance of AC line M-N	0.6255Ω/km
Equivalent impedance of AC system S_1	$4.477 + j59.913\Omega$
Zero-sequence impedance of AC system S_1	$2.0 + j6.37\Omega$

4.2 | Simulation results of in-zone fault on AC line via different fault resistances

When there is no fault in AC/DC hybrid system, Y-bridge and D-bridge converters can commutate normally. Suppose at $t = 0$ ms, VTY_1 and VTY_2 of Y-bridge converter and VTD_1 and VTD_2 of D-bridge converter are conducted. After firing signals are issued to VTY_3 of Y-bridge converter and VTD_3 of D-bridge converter, commutation will take place in Y-bridge converter and D-bridge converter. When the voltage that VTD_1 of D-bridge converter bears first turns from negative to positive and the blocking capability of VTD_1 is restored, the commutation in Y-bridge converter and D-bridge converter is finished. In the new conducting state, VTY_2 and VTY_3 of Y-bridge converter and VTD_2 and VTD_3 of D-bridge converter are conducted.

Phase-A-to-ground fault and phase-AB-to-ground fault are set at 50% line length from bus M on AC line M-N with the fault resistance ranging between 0Ω and 300Ω. At $t = 0$ ms, VTY_1 and VTY_2 of Y-bridge converter and VTD_1 and VTD_2 of D-bridge converter are conducted. After firing signals are issued to VTY_3 of Y-bridge converter and VTD_3 of D-bridge converter, commutation will take place in Y-bridge converter and D-bridge converter. When the voltage that VTD_1 of D-bridge converter bears first turns from negative to positive, the conducting states of Y-bridge converter and D-bridge converter are shown in Table 2.

It can be seen from Table 2 that, when phase-A-to-ground fault occurs on AC line with the fault resistance being 50Ω, VTD_2 and VTD_3 of D-bridge converter are conducted, while VTY_1 and VTY_2 of Y-bridge converter are conducted, which is abnormal, that is, commutation failure occurs in Y-bridge converter. When the fault resistance of phase-A-to-ground fault varies between 150Ω and 300Ω, the conducting states of converters are the same as in normal operation state, that is, both

TABLE 2 Conducting states of converters when phase-A-to-ground fault and phase-AB-to-ground fault occur via different fault resistances

Fault resistance (Ω)	Conducted valves	
	Phase-A-to-ground fault	Phase-AB-to-ground fault
0	VTY_1, VTY_2, VTD_1, VTD_2	VTY_1, VTY_2, VTD_1, VTD_2
50	VTY_1, VTY_2, VTD_2, VTD_3	VTY_1, VTY_2, VTD_2, VTD_3
100	VTY_1, VTY_2, VTD_2, VTD_3	VTY_2, VTY_3, VTD_2, VTD_3
150	VTY_2, VTY_3, VTD_2, VTD_3	VTY_2, VTY_3, VTD_2, VTD_3
200	VTY_2, VTY_3, VTD_2, VTD_3	VTY_2, VTY_3, VTD_2, VTD_3
250	VTY_2, VTY_3, VTD_2, VTD_3	VTY_2, VTY_3, VTD_2, VTD_3
300	VTY_2, VTY_3, VTD_2, VTD_3	VTY_2, VTY_3, VTD_2, VTD_3

Y-bridge converter and D-bridge converter commutate normally. When phase-AB-to-ground fault occurs, similar analysis procedure is applied, and it can be seen from Table 2 that, when the fault resistance varies between 0Ω and 50Ω, commutation failure occurs; when the fault resistance varies between 100Ω and 300Ω, both Y-bridge converter and D-bridge converter commutate normally.

Concerning the above two fault types, whether commutation failure occurs in inverter-side converter station or not, this paper constructs the topology of inverter-side network that can reflect the actual conducting states of converter valves. Thus the fault location calculated according to (44) is the actual fault location, and the fault likeness factor calculated according to (48) is bigger than the threshold value. The signals of voltage and current are shown in Figure 10, and the fault resistances are 300Ω. The calculated fault location and fault likeness factor corresponding to the above two fault types are shown in Figure 10.

It can be seen from Figure 10(c) and (g) that the calculation results of fault location in different fault cases are all close to 50%. The relative locating error slightly fluctuates as the fault resistance increases, but remains below 0.18%, thus the locating result is accurate. The locating error mainly comes from substituting the differential method with difference method.

It can be seen from Figure 10(d) and (h) that, in different fault cases, as the fault resistance increases, the values of fault likeness factors at the same time section all decrease. When phase-A-to-ground fault occurs with the fault resistance being 300Ω, the fault likeness factor first increases and then decreases as the time window slides, as shown in Figure 10(d). The minimum value of fault likeness factor 38.21 appears at $t = 3.85$ ms, which is much larger than the threshold value. When phase-AB-to-ground fault occurs with the fault resistance being 300Ω, the minimum value of fault likeness factor 44.51 appears at $t = 4$ ms, as shown in Figure 10(h).

According to Figure 10, concerning the above two fault types, the calculated fault location is consistent with the actual fault location, and the fault likeness factor is bigger than the threshold value. Thus the fault is identified to be at 50% line length from bus M on AC line M-N, and distance protection will operate correctly. Based on the above analysis, when in-zone fault occurs on AC line via different fault resistances, the proposed scheme is highly sensitive and can quickly identify the fault, unaffected by the commutation failure and fault type.

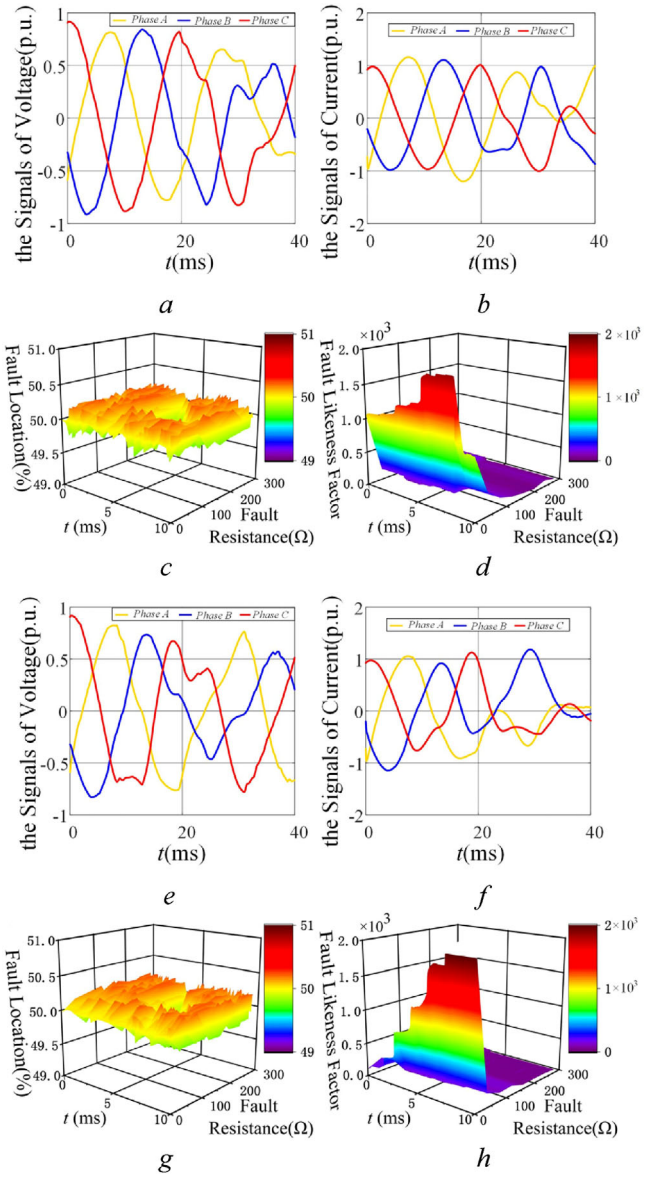

FIGURE 10 Fault location and fault likeness factor when phase-A-to-ground fault and phase-AB-to-ground fault occur on AC line via different fault resistances: (a) the signals of voltage in the case of phase-A-to-ground fault,(b) the signals of current in the case of phase-A-to-ground fault, (c) fault location in the case of phase-A-to-ground fault,(d) fault likeness factor in the case of phase-A-to-ground fault, (e) the signals of voltage in the case of phase-AB-to-ground fault,(f) the signals of current in the case of phase-AB-to-ground fault, (g) fault location in the case of phase-AB-to-ground fault and (h) fault likeness factor in the case of phase-AB-to-ground fault

4.3 | Simulation results of in-zone fault at different locations on AC line

Phase-A-to-ground fault and phase-A-to-phase-B fault are set at different locations on AC line, and the fault resistance of phase-A-to-ground fault is 300Ω. At $t = 0$ ms, VTY_1 and VTY_2

TABLE 3 Conducting states of converters when phase-A-to-ground fault and phase-A-to-phase-B fault occur at different locations on AC line

	Conducted valves	
Fault location	**Phase-A-to-ground fault**	**Phase-A-to-phase-B fault**
20%	VTY_1, VTY_2, VTD_1, VTD_2	VTY_1, VTY_2, VTD_2, VTD_3
40%	VTY_1, VTY_2, VTD_2, VTD_3	VTY_1, VTY_2, VTD_2, VTD_3
60%	VTY_2, VTY_3, VTD_2, VTD_3	VTY_1, VTY_2, VTD_2, VTD_3
80%	VTY_2, VTY_3, VTD_2, VTD_3	VTY_1, VTY_2, VTD_2, VTD_3
95%	VTY_2, VTY_3, VTD_2, VTD_3	VTY_1, VTY_2, VTD_2, VTD_3

of Y-bridge converter and VTD_1 and VTD_2 of D-bridge converter are conducted. After firing signals are issued to VTY_3 of Y-bridge converter and VTD_3 of D-bridge converter, commutation will take place in Y-bridge converter and D-bridge converter. When the voltage that VTD_1 of D-bridge converter bears first turns from negative to positive, the conducting states of Y-bridge converter and D-bridge converter are shown in Table 3.

It can be seen from Table 3 that, when phase-A-to-phase-B fault occurs at any location on AC line, the blocking capability of VTY_1 in Y-bridge converter cannot be restored when it bears reverse voltage, thus it can be identified that commutation failure occurs in Y-bridge converter. After the commutation from VTD_1 to VTD_3 of D-bridge converter is finished, VTD_2 and VTD_3 of D-bridge converter are conducted, and VTY_1 and VTY_2 of Y-bridge converter are conducted. Similarly, it can be identified that, when phase-A-to-ground fault occurs with the fault location varying between 20% and 40%, commutation failure occurs; when the fault location varies between 60% and 95%, both Y-bridge converter and D-bridge converter commutate normally.

In the above two fault cases, this paper constructs the equivalent circuit of inverter station that can reflect the actual conducting states of converter valves, thus whether commutation failure occurs in inverter-side converter station or not, the fault location calculated according to (44) is the actual fault location, and the fault likeness factor calculated according to (48) is bigger than the threshold value. The signals of voltage and current are shown in Figure 11, and the actual fault locations are at 80% of AC line M-N. The calculated fault location and fault likeness factor in the above two fault cases are shown in Figure 11.

It can be seen from Figure 11(c) and (g) that the simulation results of actual fault distance percentage and the calculated fault location form a 45° slanted plane, it means the actual fault distance and the calculated fault location at different time sections are consistent, and the locating error increases as the actual fault distance increases. When phase-A-to-ground fault occurs at 90% line length from bus M, the relative locating error reaches the maximum value 0.16%.

It can be seen from Figure 11(d) and (h) that, the fault likeness factors in different fault cases are bigger than the threshold value, which is consistent with the conclusion of Table 3. When fault occurs at any location on AC line, as the actual fault distance percentage increases, the fault likeness factors at the same time section first increase and then decrease. When phase-A-to-ground fault occurs at 40% line length from bus M, the minimum value of fault likeness factor 27.11 appears at $t = 3.85$ ms, as shown in Figure 11(d). When phase-A-to-phase-B fault occurs at 90% line length from bus M, the minimum value of fault likeness factor 80.37 appears at $t = 0$ ms, as shown in Figure 11(h).

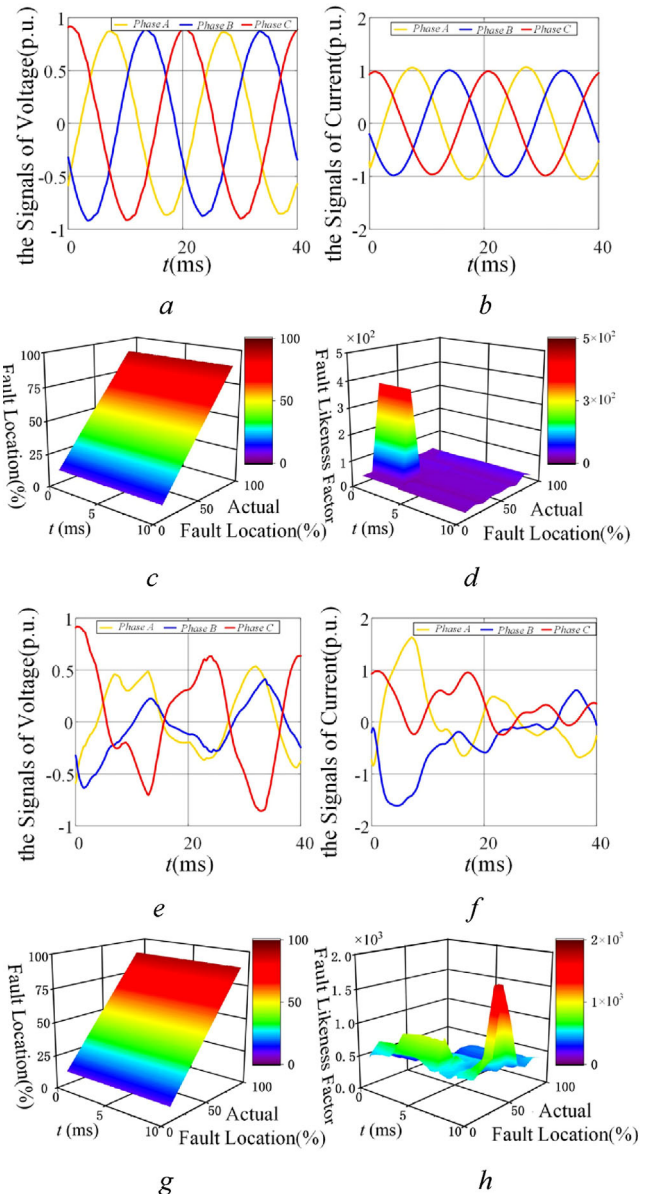

FIGURE 11 Fault location and fault likeness factor when phase-A-to-ground fault and phase-A-to-phase-B fault occur at different locations on AC line: (a) the signals of voltage in the case of phase-A-to-ground fault,(b) the signals of current in the case of phase-A-to-ground fault, (c) fault location in the case of phase-A-to-ground fault,(d) fault likeness factor in the case of phase-A-to-ground fault, (e) the signals of voltage in the case of phase-A-to-phase-B fault,(f) the signals of current in the case of phase-A-to-phase-B fault, (g) fault location in the case of phase-A-to-phase-B fault and (h) fault likeness factor in the case of phase-A-to-phase-B fault

TABLE 4 Conducting states of converters when phase-A-to-ground fault occurs at f_1

Fault resistance (Ω)	Conducted valves
0	VTY_1, VTY_2, VTD_2, VTD_3
50	VTY_2, VTY_3, VTD_2, VTD_3
100	VTY_2, VTY_3, VTD_2, VTD_3
150	VTY_2, VTY_3, VTD_2, VTD_3
200	VTY_2, VTY_3, VTD_2, VTD_3
300	VTY_2, VTY_3, VTD_2, VTD_3

In the above fault cases, the calculated fault locations are the same as the actual fault locations, and the fault likeness factors are all bigger than the threshold value, thus they are identified as in-zone faults on AC line M-N, and distance protection will operate correctly. According to the above analysis, the proposed protection criterion is not affected by the fault location and commutation failure, and is highly sensitive even to fault at the end of line.

4.4 | Simulation results of fault in DC system on the backside of AC line

Phase-A-to-ground fault is set at f_1 in Figure 1 with the fault resistance ranging between 0Ω and 300Ω. At $t = 0$ ms, VTY_1 and VTY_2 of Y-bridge converter and VTD_1 and VTD_2 of D-bridge converter are conducted. After firing signals are issued to VTY_3 of Y-bridge converter and VTD_3 of D-bridge converter, commutation will take place in Y-bridge converter and D-bridge converter. When the voltage that VTD_1 of D-bridge converter bears first turns from negative to positive, the conducting states of Y-bridge converter and D-bridge converter are shown in Table 4.

It can be seen from Table 4 that, when the fault resistance is 0Ω, the blocking capability of VTY_1 in Y-bridge converter cannot be restored when it bears reverse voltage, thus commutation failure occurs in Y-bridge converter. When the fault resistance varies between 50Ω and 300Ω, the conducting states of Y-bridge converter and D-bridge converter are the same as in normal operation state, thus Y-bridge converter and D-bridge converter both commutate normally.

In the above fault case, since the fault point is at f_1 in DC system, (44) is not satisfied, and the fault likeness factor calculated according to (48) is smaller than the threshold value. The signals of voltage and current are shown in Figure 11, and the fault resistances are 10Ω. The calculated fault likeness factor is shown in Figure 12.

It can be seen from Figure 12(c) that, in this fault case, as the fault resistance increases, the fault likeness factors at different time sections fluctuate slightly but remain below the threshold value. According to Figure 12(d), when the fault resistance is 0 Ω, the maximum value of fault likeness factor 0.11 appears at $t = 3.45$ ms, which is much smaller than the threshold value, thus no in-zone fault on AC line M-N is identified, and distance protection will not operate. According to the above analysis, the proposed protection criterion can correctly distinguish between in-zone and out-of-zone faults, unaffected by the commutation failure.

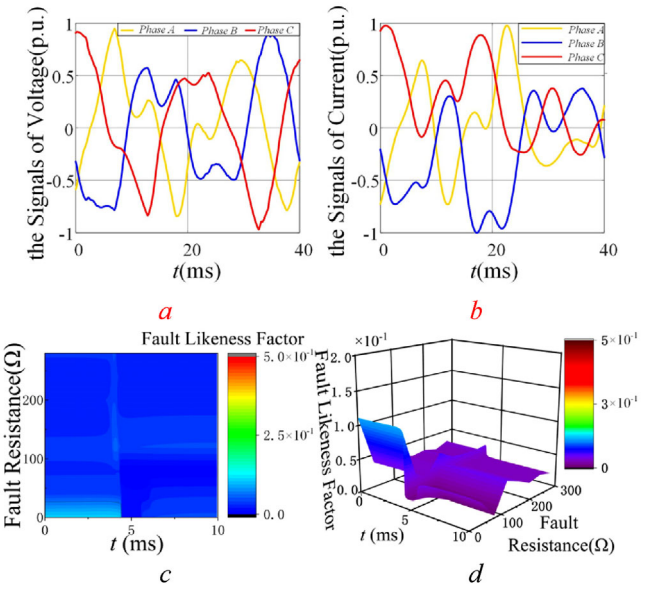

FIGURE 12 Fault likeness factor when phase-A-to-ground fault occurs at f_1: (a) the signals of voltage in the case of phase-A-to-ground fault,(b) the signals of current in the case of phase-A-to-ground fault, (c) fault location in the case of phase-A-to-ground fault and (d) fault likeness factor in the case of phase-A-to-ground fault

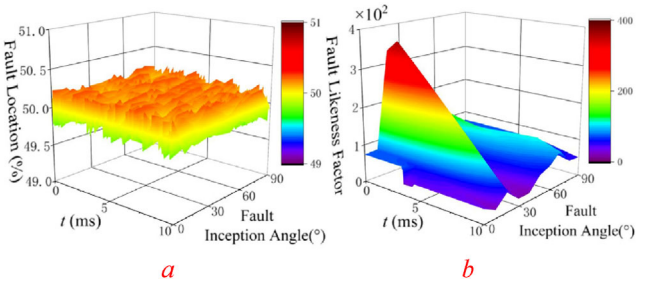

FIGURE 13 Variation of fault location and fault likeness factor with the fault inception angle: (a) fault location in the case of phase-A-to-ground fault and (b) fault likeness factor in the case of phase-A-to-ground fault

4.5 | Simulation verification of the proposed method regarding varying fault inception angle, window size and sampling frequency

Phase-A-to-ground fault is set at 50% line length from bus M on AC line M-N, with the fault resistance being 300Ω. When the window size is 10 ms, the sampling frequency is 10 kHz, and the fault inception angle varies from 0 to 90°, the variation of fault location and fault likeness factor is shown in Figure 13.

It can be seen from Figure 13 that, as the fault inception angle increases, fault likeness factor at the same time section first increases and then decreases, while the relative error of fault

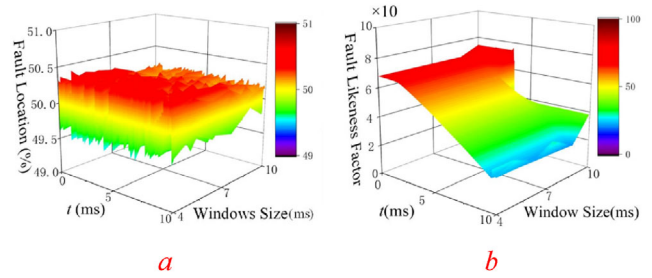

FIGURE 14 Variation of fault location and fault likeness factor with the window size: (a) fault location in the case of phase-A-to-ground fault and (b) fault likeness factor in the case of phase-A-to-ground fault

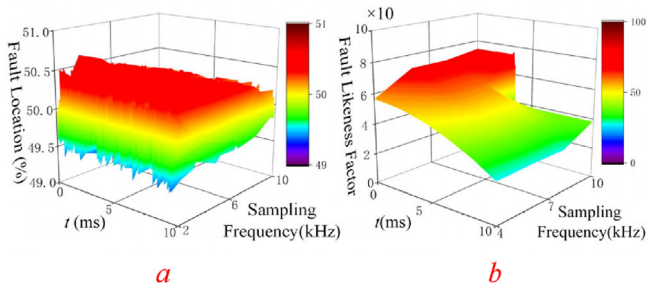

FIGURE 15 Variation of fault location and fault likeness factor with the sampling frequency: (a) fault location in the case of phase-A-to-ground fault and (b) fault likeness factor in the case of phase-A-to-ground fault

locating fluctuates modestly. According to Figure 13(a), when the fault inception angle is 60°, the relative error of fault locating reaches the maximum value 0.17% at $t = 4.45$ ms. As shown in Figure 13(b), when the fault inception angle is 0°, fault likeness factor reaches the minimum value 18.49 at $t = 9.95$ ms.

When the fault inception angle is 0°, the sampling frequency is 10 kHz, and the window size varies from 4 to 10 ms, the variation of fault location and fault likeness factor is shown in Figure 14.

It can be seen from Figure 14 that, as the window size increases, the relative error of fault locating at the same time section keeps decreasing, while fault likeness factor keeps increasing. In Figure 14(a), when the window size is 4 ms, the relative error of fault locating reaches the maximum value 0.99% at $t = 1.35$ ms. In Figure 14(b), when the window size is 5 ms, fault likeness factor reaches the minimum value 20.82 at $t = 9.9$ ms.

When the fault inception angle is 0°, the window size is 10 ms, and the sampling frequency varies from 4 to 10 kHz, the variation of fault location and fault likeness factor is shown in Figure 15.

It can be seen from Figure 15(a) and (b) that, as the sampling frequency increases, the relative error of fault locating at the same time section keeps decreasing, while fault likeness factor keeps increasing. According to Figure 15(a), when the sampling frequency is 4 kHz, the relative error of fault locating reaches the maximum value 1.2% at $t = 6.8$ ms. In Figure 15(b), when the sampling frequency is 4 kHz, the fault likeness factor reaches the minimum value 26.69 at $t = 9.9$ ms.

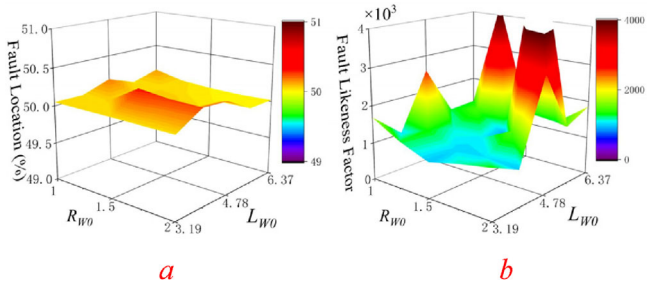

FIGURE 16 Fault location and fault likeness factor in the case of phase-A-to-ground fault: (a) fault location in the case of phase-A-to-ground fault and (b) fault likeness factor in the case of phase-A-to-ground fault

Based on the above analysis, the proposed protection criterion is not affected by the variation of fault inception angle. Even when the sampling frequency is relatively low and the window size is relatively small, the proposed scheme can still correctly and reliably identify in-zone and out-of-zone faults.

4.6 | The impact of R_{W0} and L_{W0} on the performance of the proposed protection scheme

Phase-A-to-ground fault is set at 50% line length from bus M on AC line M-N, with the fault resistance being 100Ω and zero-sequence impedance varying from $1.0 + j3.19\Omega$ to $2.0 + j6.37\Omega$. In this case, the variation of fault location and fault likeness factor is shown in Figure 16.

It can be seen from Figure 16(a) that, as zero-sequence impedance varies, the calculated results of fault location remain close to 50%, with the relative error of fault locating fluctuating slightly. When zero-sequence impedance is $1.4 + 3.822\Omega$, the relative error of fault locating reaches the maximum value 0.18%, thus the locating result is relatively accurate. According to Figure 16(b), as zero-sequence impedance varies, fault likeness factor remains above the operation threshold value. When zero-sequence impedance is $1.4 + 5.096\Omega$, fault likeness factor reaches the minimum value 873.71, which is much larger than the operation threshold value. Thus it is correctly identified as in-zone fault on AC line M-N, and the protection will operate.

Based on the above analysis, the proposed protection criterion can correctly distinguish between in-zone and out-of-zone faults, and is scarcely affected by the variation of zero-sequence impedance of inverter-side AC system.

4.7 | The applicability of the proposed protection scheme in large AC/DC hybrid system

To verify the applicability of the proposed protection scheme in large AC/DC hybrid system, simulation tests are conducted on RT-LAB platform. The structure of test system is shown in Figure 17, where the receiving-end AC system uses IEEE 39-bus system, and DC system applies CIGRE HVDC standard model.

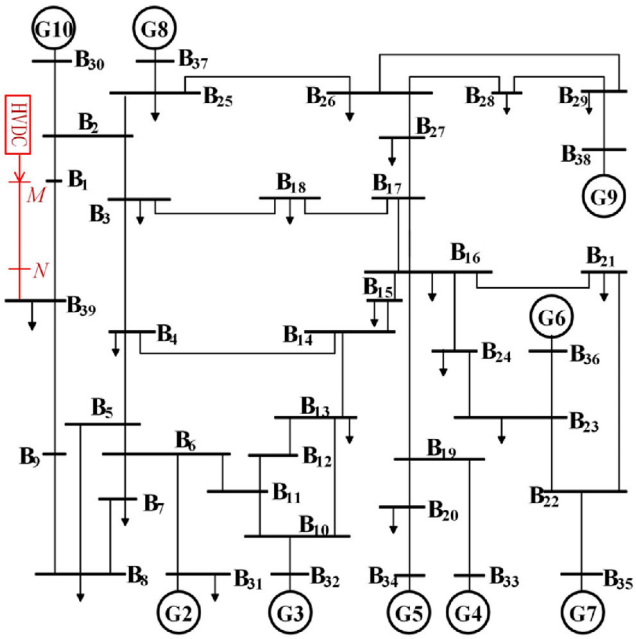

FIGURE 17 Large AC/DC hybrid system

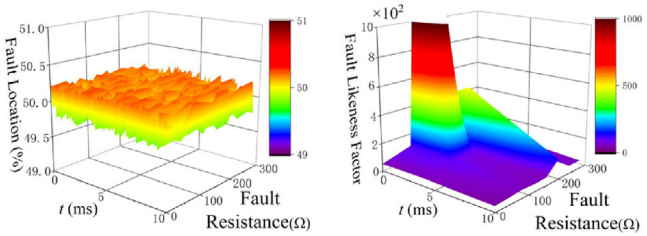

FIGURE 18 Variation of fault location and fault likeness factor when phase-A-to-ground fault occurs via different fault resistances: (a) fault location in the case of phase-A-to-ground fault and (b) fault likeness factor in the case of phase-A-to-ground fault

Phase-A-to-ground fault is set at 50% line length from bus M on AC line M-N, with the fault resistance varying between 0Ω and 300Ω. In such fault case, the variation of fault location and fault likeness factor is shown in Figure 18.

According to Figure 18(a), as the fault resistance varies, the calculated results of fault location remain close to 50%, with the relative error of fault locating fluctuating slightly. When the fault resistance is 80Ω, the relative error of fault locating reaches the maximum value 0.5% at $t = 1.8$ ms. Thus, the locating result is relatively accurate.

It can be seen from Figure 18(b) that, as the fault resistance increases, fault likeness factor at different time sections first increases and then decreases, but it remains above the operation threshold value. When the fault resistance is 0Ω, fault likeness factor reaches the minimum value 40.51 at $t = 9.95$ ms, which is much larger than the operation threshold value. Thus it is identified as in-zone fault, and protection will operate correctly.

Phase-A-to-ground fault is set at different locations within the protection zone of AC line, with the fault resistance being

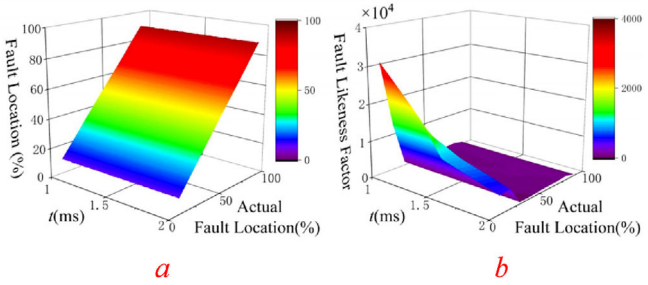

FIGURE 19 Variation of fault location and fault likeness factor when phase-A-to-ground fault occurs at different locations: (a) fault location in the case of phase-A-to-ground fault and (b) fault likeness factor in the case of phase-A-to-ground fault

300Ω. In such fault case, the variation of fault location and fault likeness factor is shown in Figure 19.

It can be seen from Figure 19(a) that, a 45° inclined plane is formed by the axes of time, actual fault location and calculated fault location. It means the calculated fault location is consistent with the actual fault location at different time sections, and the relative error of fault locating increases as the actual fault distance increases. When phase-A-to-ground fault occurs at 90% line length from bus M, the relative error of fault locating reaches the maximum value 0.25% at $t = 0.8$ ms.

According to Figure 19(b), in different fault cases, fault likeness factor remains above the threshold value. As the actual fault distance increases, fault likeness factor at the same time section keeps decreasing. When phase-A-to-ground fault occurs at 90% line length from bus M, fault likeness factor reaches the minimum value 26.18 at $t = 9.9$ ms.

Based on the above analysis, the proposed protection criterion is applicable to large AC/DC hybrid system, with relatively high sensitivity and fast identification capability.

5 | CONCLUSION

Concerning the mal-operation of distance protection in AC/DC hybrid system due to commutation failure caused by AC-side fault, a novel AC line distance protection scheme based on fault likeness factor is put forward, which can solve problems in traditional distance protection caused by commutation failure, such as narrowed protection range and over-reach operation. The proposed scheme has the following characteristics.

1. The time-varying model of AC/DC hybrid system considering the dynamic process of commutation failure is built, which can simultaneously reflect the current conducting state of inverter valves and AC-side fault state. Thus, the inaccuracy of fault model in traditional method caused using controlled source to represent DC system can be avoided.
2. The proposed method takes into account non-linear transient characteristics of fault currents, and uses the instantaneous values instead of the phasor values of fault currents to calculate fault parameters in the time-varying model, thus the accuracy of fault locating is high.

3. The proposed scheme can correctly and reliably identify in-zone and out-of-zone faults when commutation failure is caused by different types of fault at different locations.
4. When fault occurs at the outlet of AC line backside system, the protection does not operate. Even when the zero-sequence network of receiving-end AC system varies, the proposed method can still correctly identify the fault location.
5. The proposed scheme is strongly immune to fault resistance, and is highly sensitive even to high-resistance fault at line end.

ACKNOWLEDGEMENTS

This work was supported by National Natural Science Foundation of China (51822703) and Chinese Universities Scientific Fund (2018JQ01, 2018ZD01).

REFERENCES

1. Abdulrahman, A., et al.: HVDC transmission: technology review, market trends and future outlook. Renewable Sustainable Energy Rev. 112, 530–554 (2019)
2. Long, W., Nilsson, S., HVDC transmission: yesterday and today. IEEE Power Energ. Mag. 8(2), 22–31 (2007)
3. Javad, K., et al.: Review of HVDC control in weak AC grids. Electr. Power Syst. Res. 162, 194–206 (2018)
4. Yang, H.H., et al.: A novel assessment index of LCC-HVDC system impact on short-term voltage stability of the receiving-end AC system. IEEE Trans. Power Delivery 142, 125–133 (2017)
5. Son, H.I., Kim, H.M., An algorithm for effective mitigation of commutation failure in high-voltage direct-current systems. IEEE Trans. Power Delivery 31(4), 1437–1446 (2016)
6. Luo, S.B., et al.: Non-unit transient based boundary protection for UHV transmission lines. Int. J. Electr. Power Energy Syst. 102, 349–363 (2018)
7. Zheng, J.C., et al.: A novel differential protection scheme for HVDC transmission lines. Int. J. Electr. Power Energy Syst. 94, 171–178 (2018)
8. Vazquez, E., et al.: A new approach traveling-wave distance protection – part I: algorithm. IEEE Trans. Power Delivery 22(2), 795–800 (2007)
9. Shehab-Eldin, E.H., Mclaren, P.G., Travelling wave distance protection-problem areas and solutions. IEEE Trans. Power Delivery 3(3), 894–902 (2007)
10. Vitins, M., A correlation method for transmission line protection. IEEE Trans. Power Appar. Syst. PAS-97(5), 1607–1617 (1978)
11. Ma, J., et al.: An adaptive distance protection scheme based on the voltage drop equation. IEEE Trans. Power Delivery 30(4), 1931–1940 (2015)
12. Ma, J., et al.: A novel adaptive distance protection scheme for DFIG wind farm collector lines. Int. J. Electr. Power Energy Syst. 94, 234–244 (2018)
13. Rahimi, E., et al.: Commutation failure analysis in multi-infeed HVDC systems. IEEE Trans. Power Delivery 26(1), 378–384 (2011)
14. Kristmundsson, G.M., Carroll, D.P., The effect of AC system frequency spectrum on commutation failure in HVDC inverters. IEEE Trans. Power Delivery 5(2), 1121–1128 (1990)
15. Thio, C.V., et al.: Commutation failures in HVDC transmission systems. IEEE Trans. Power Delivery 11(2), 946–957 (1996)
16. Huang, S.F., et al.: Effect of commutation failure on the distance protection and the countermeasures. IET Gener. Transm. Distrib. 9(9), 838–844 (2015)
17. Wang, D., Hou, M., Novel pilot protection for AC transmission line connected to LCC-HVDC inverter station. Int. J. Electr. Power Energy Syst. 108, 347–358 (2019)
18. Zhu, Y.N., et al.: Prevention and mitigation of high-voltage direct current commutation failures: a review and future directions. IET Gener. Transm. Distrib. 13(24), 5449–5456 (2019)
19. Segui, T., et al.: Fundamental basis for distance relaying with parametrical estimation. IEEE Trans. Power Delivery 15(2), 659–664 (2000)

How to cite this article: Ma J, Wu Y, Phadke AG. A novel AC line distance protection scheme for AC/DC hybrid system based on fault likeness factor. *IET Gener Transm Distrib.*2021;15:912–926.
https://doi.org/10.1049/gtd2.12068